Pulse Arrival Time Segmentation into Cardiac and Vascular Intervals – Implications for Pulse Wave Velocity and Blood Pressure Estimation

[1,2]Fabian Beutel, [1,2,3]Chris Van Hoof, [3]Xavier Rottenberg, [4]Koen Reesink, [2]Evelien Hermeling

Abstract— Objective: **This study demonstrates a novel method for pulse arrival time (PAT) segmentation into cardiac isovolumic contraction (IVC) and vascular pulse transit time to approximate central pulse wave velocity (PWV).** *Methods:* **10 subjects (38±10 years, 121±12 mmHg SBP) ranging from normotension to hypertension were repeatedly measured at rest and with induced changes in blood pressure (BP), and thus PWV. ECG was recorded simultaneously with ultrasound-based carotid distension waveforms, a photoplethysmography-based peripheral waveform, noninvasive continuous and intermittent cuff BP. Central PAT was segmented into cardiac and vascular time intervals using a fiducial point in the carotid distension waveform that reflects the IVC onset. Central and peripheral PWVs were computed from (segmented) intervals and estimated arterial path lengths. Correlations with Bramwell-Hill PWV, systolic and diastolic BP (SBP/DBP) were analyzed by linear regression.** *Results:* **Central PWV explained more than twice the variability (R^2) in Bramwell-Hill PWV compared to peripheral PWV (0.56 vs. 0.27). SBP estimated from central PWV undercuts the IEEE mean absolute deviation threshold of 5 mmHg, significantly lower than peripheral PWV or PAT (4.2 vs. 7.1 vs. 10.1 mmHg).** *Conclusion:* **Cardiac IVC onset signaled in carotid distension waveforms enables PAT segmentation to obtain unbiased vascular pulse transit time. Corresponding PWV estimates provide the basis for single-site assessment of central arterial stiffness, confirmed by significant correlations with Bramwell-Hill PWV and SBP.** *Significance:* **In a small-scale cohort, we present proof-of-concept for a novel method to estimate central PWV and BP, bearing potential to improve the practicality of cardiovascular risk assessment in clinical routines.**

Index Terms— **Algorithms, Biomarkers, Biomedical signal processing, Biomedical transducers, Electrocardiography, Patient monitoring, Sensor fusion, Ultrasonography.**

I. INTRODUCTION

A. Pulse Wave Velocity – An Independent Cardiovascular Risk Marker, Depending on Blood Pressure

Increased arterial stiffness is a recognized risk marker in addition to elevated blood pressure (BP), and even considered as crucial precursor of hypertension [1]. Arterial stiffness can be assessed by measuring the arterial pulse wave velocity (PWV), which has been shown to be an independent predictor of cardiovascular disease, all-cause mortality and treatment prognosis [2], [3] as well as incident hypertension [4].

The biomechanical relation between PWV and arterial stiffness may be expressed by the equations of Moens-Korteweg [5], linking PWV to Young's elastic modulus, or Bramwell-Hill (Eq.1) [6], linking PWV to blood density ρ and wall distensibility, i.e. the relative change in volume V (or cross-sectional area A) per change in pressure P.

$$PWV = \sqrt{\frac{VdP}{\rho dV}} = \sqrt{\frac{AdP}{\rho dA}} \qquad (1)$$

Due to the nonlinear pressure-volume relation of the arterial wall, PWV inherently depends on BP and may therefore be used for its estimation. Wall stiffness increases exponentially from diastolic (DBP) to systolic BP (SBP), as wall stress is transferred from elastic to stiffer structural components [7]. Human arteries exhibit heterogenous properties from central elastic conduit to peripheral muscular arteries, the latter whose stiffness is not only intrinsically higher but also modulated by vascular smooth muscle tone [8], [9].

B. State of the Art Pulse Wave Velocity Measures

The clinical gold-standard is the carotid-femoral PWV, calculated as

$$PWV = \frac{L}{PTT} \qquad (2)$$

from an estimated distance L between the respective arterial sites and the pulse transit time (PTT) elapsing between fiducial markers of the local pressure waveforms (Fig. 1). The carotid-femoral PWV was recently re-evaluated and found superior in estimating central aortic stiffness compared to methods involving peripheral arterial pathways or cuffs with population based transfer functions [10]. However, in spite of its predictive utility, the recommended use of PWV in hypertension management guidelines was downgraded for reasons of impracticality in clinical routines [11], [12].
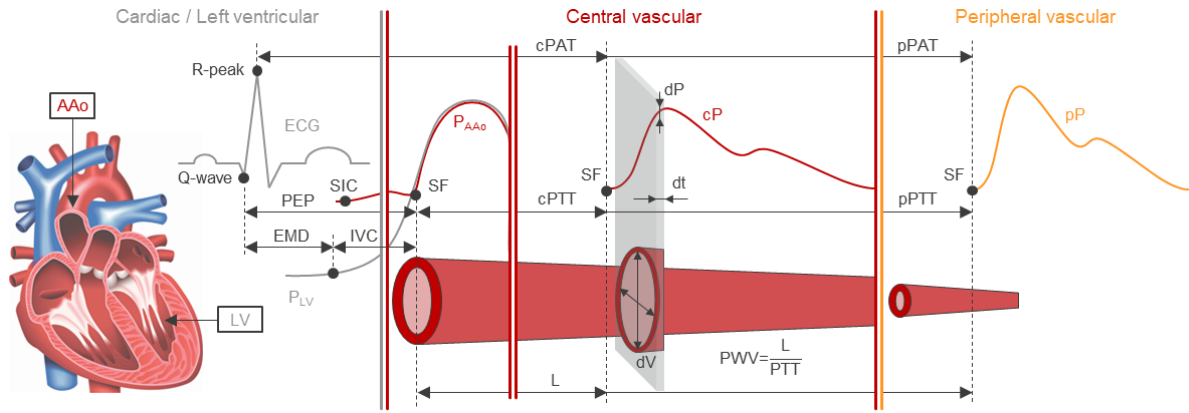
Fig. 1. Concepts of pulse wave propagation. Cardiac, left ventricular, central-, and peripheral vascular time intervals (in sequence from left to right). Illustration of pulse arrival time, pulse transit time and corresponding arterial path length for pulse wave velocity computation. Grey slice highlighting incremental pressure-volume changes for local pulse wave velocity computation. Note that for illustration purposes time axis is not consistent.

AAo = ascending aorta / aortic (subscript); c = central (prefix); DBP = diastolic blood pressure; ECG = electrocardiogram; EMD = electromechanical delay; IVC = isovolumic contraction; L = arterial segment length; LV = left ventricle / ventricular (subscript); p = peripheral (prefix); P = pressure; PAT = pulse arrival time; PEP = pre-ejection period; PTT = pulse transit time; PWV = pulse wave velocity; SF = systolic foot; SBP = systolic blood pressure; SIC = start of isovolumic contraction; V = volume.

Local PWV measures come with different challenges, e.g. they require invasive or less accessible imaging modalities to compute local distensibility and are susceptible to complex wave reflections [13], [14]. In contrast, Eq.2 laid the foundation for the more simplistic pulse arrival time (PAT) based approaches, which have been a subject of broad scientific interest for BP estimation throughout the past decade [15]–[19]. While PTT commonly refers to the actual vascular transit time, pulse arrival time (PAT) refers to the interval between the electrocardiogram (ECG) R-peak and the systolic foot (SF) identified in a peripheral pressure waveform (Fig. 1), typically acquired by photoplethysmography (PPG).

C. Strengths & Drawbacks of Pulse Arrival Time

On the one hand, PAT-based approaches allow for cheap and user-friendly integration in wearables or portable devices such as smartphone, patch or weighing scale [20]–[22] and offer significant correlations with BP, irrespective of simple regression techniques or machine learning approaches with secondary predictors [19]. On the other hand, PAT-based approaches suffer from three decisive drawbacks in view of their fundamental relation with PWV and hence BP.

Firstly, they mostly involve peripheral arterial pathways of heterogeneous and locally modulated stiffness, hence confounding the PWV estimated from PAT. Intra-subject changes in arterial stiffness are known to occur frequently and affect the PAT-BP relation, such that intermittent cuff calibrations are required for proper BP estimation, even for invasive PAT measurements from the radial artery [23].

Secondly, the prevailing PPG sensors yield quasi-volumetric waveforms, which are subject to local microvascular perfusion and may lead to biased fiducial points signaling the wave arrival. In contrast, ultrasound imaging would allow for deeper tissue penetration and enable spatial resolution to monitor actual arterial distension, particularly in miniaturized devices [24]. However, a comparative performance evaluation between central ultrasound-based and peripheral PPG waveforms in PAT-based approaches has not yet been performed.

Thirdly, unlike PTT, PAT is significantly biased by the cardiac pre-ejection period (PEP) prior to the aortic valve opening. The PEP comprises an electromechanical delay (EMD) between early depolarization, marked by the ECG Q-wave, and the subsequent isovolumic contraction (IVC) of the left ventricle (Fig. 1), such that

$$PAT = PEP + PTT = EMD + IVC + PTT. \qquad (3)$$

With EMD assumed constant at 30-40 ms within subjects and insensitive to physiological states [25], PEP is largely determined by IVC, expected to be 40 ms on average and highly sensitive to sympathetic activity and pressure-dependent cardiac regulation [26], [27]. Since the role of PAT as an inadequate marker of PTT for BP estimation was established by invasive studies [28], [29], more recent research aimed at measuring PEP noninvasively by means of impedance cardiography [22], [30], ballistocardiography [31], seismocardiography [21] or on-body radar [32], [33]. These approaches, however, require additional sensing modalities with varying accuracy for PEP [34].

Interestingly, IVC was also found to be evident in central ultrasound distension waveforms, manifested as a minor pressure perturbation attributed to mechanic cardiac-aortic coupling [35], [36], whose preceding inflection is commonly referred to as start of the IVC (SIC) [26]. However, this fiducial point has never been utilized for segmentation of PAT to obtain more accurate estimations of PWV and BP.

D. Objective & Hypotheses

Key objective is to demonstrate the approximation of PWV by segmenting PAT into cardiac IVC and vascular PTT and, subsequently, to compute PWV via estimated arterial path lengths. Segmentation of PAT was done by exploiting carotid distension waveforms from ultrasound, carrying information on IVC. To provide benchmarking evidence, conventional peripheral PAT from ECG and PPG was obtained simultaneously. We hypothesized that central PTT-based

PWV is a better estimator of Bramwell-Hill PWV than PAT-based PWV, either central or peripheral.

In addition, we hypothesized that central PWV estimates, yield superior correlations with BP, contrasting the PAT-BP relation with its several dependencies. The study was designed to take into account both inter- and intra-subject variation, including normotensive and hypertensive subjects, while inducing changes in BP, and hence PWV, in repeated sessions.

II. METHODS

A. Data Collection

Data was acquired from 10 human subjects (7 male, 3 female, 38±10 years), ranging from normotension to stage 2 hypertension with mean SBP of 121±12 mmHg. All subjects gave their written informed consent. The study was reviewed by the institutional review board of the Máxima MC Hospital (Eindhoven, NL) and procedures were performed in line with good clinical practice guidelines wherever applicable in compliance with the declaration of Helsinki [37].

Fig. 2a introduces the experimental setup. Carotid artery B-mode ultrasound was recorded using a Verasonics Vantage64 (Verasonics Inc., USA) with an L11-5v linear array transducer (f_c = 7.8 MHz), acquiring a custom plane wave acquisition sequence (f_s = 500 Hz, lateral window = 19.2 mm). ECG was recorded in lead II configuration and peripheral PPG waveforms were recorded at 660 nm wavelength using the transmissive Nonin8000J probe (Nonin Medical Inc., USA) on the left index finger. The Finapres NOVA (Finapres Medical Systems B.V., NL) measured continuous BP via the volume-clamp technique on the left middle finger and intermittent BP via an oscillometric upper arm cuff. In this way, a clinically validated algorithm is deployed to reconstruct peripheral finger arterial pressure to (more central) brachial waveforms [38]. ECG, PPG and BP fed into the Biopac MP-160 base module (f_s = 500 Hz), respectively via specific modules ECG100C and PPG100C, and analog inputs (Biopac Systems Inc., USA). Verasonics and Biopac recordings were synchronized by an external trigger signal.

Fig. 2b shows a timeline of the experimental protocol. Data was collected in three repeated measurement sessions, spread over three weeks, to account for physiological intra-subject variability as well as technical measurement bias, e.g. due to sensor reattachment and probe repositioning. Demographics (gender, age, height, weight) were obtained and anthropometric distances were measured to estimate the central (L_C) and peripheral (L_P) arterial path lengths (L_C: sternal notch to common carotid artery halfway along the neck; L_P: sternal notch to left index finger). All data was recorded at constant room temperature (22°C), in supine position to eliminate the hydrostatic BP component, and with an initial resting phase of 10 minutes to bring hemodynamics and vasomotor tone as close as possible to baseline [39]. Each session, in turn, comprised three interventions. First, 2 minutes in resting condition were recorded for best inter-subject comparability. Second, the subject was asked to perform 2 minutes of paced breathing to induce cyclic BP variation at 7.5 cycles per minute, guided by an acoustic reference signal. Third, to induce a short-term gradual BP increase, the subject was asked to perform a hand grip dynamometer exercise with the sensor free hand for 1 minute at maximal voluntary contraction, followed by 1 minute of recovery. Continuous BP was obtained throughout the interventions for detailed investigation of relative changes and intermittent cuff BP as gold standard measure pre-, and post resting and hand grip.

B. Data Processing & Statistical Analysis

Fig. 2c shows a flow diagram of the post-processing and analysis conducted in Matlab 2018a (Mathworks Inc., USA).

1) Beamforming & Arterial Wall Tracking

Initially, the raw ultrasound radio frequency (RF) data matrix (x = 64 scanlines = 19.2 mm, y = 1024 depth samples = 24.6 mm, z = 5000 frames = 10 s, per block) was delay-and-sum beamformed using the Matlab Phased Array System Toolbox 2018a (Mathworks Inc., USA) specified for the L11-5v transducer characteristics [40]. The beamformed and size-preserved RF matrix was further processed by an ECG-gated wall tracking algorithm to obtain arterial distension timeseries signals [41]. In more detail, the wall tracking algorithm comprises an automated wall position detection triggered by the ECG R-peak [42]. Starting from the detected wall position, wall motion is tracked throughout the cardiac cycle, via complex cross-correlation of a Hilbert-transformed, depth-, and time-shifted submatrix (kernel: x = 2 scanlines = 0.6 mm, y = 50 depth samples = 1.2 mm, z = 5 frames = 10 ms). Differential motion of the anterior and posterior arterial wall eventually yielded a total of 32 distension waveforms as motion was averaged per 2 adjacent scanlines.

2) Feature Extraction & Qualification

From the filtered ECG signal, R-peaks were detected using Matlab function *findpeaks*. All pulse waveform signals (BP, distension and PPG) were passed through a second-order low-pass filter with cut-off frequency 40 Hz for high-frequency noise removal. To obtain the first derivative (dt), the signals were passed through a simple derivative filter (kernel: [1 -1]). For the second derivative (d2t), Matlab function *filtfilt* was used to pass the signals through a cascaded first-order high-pass filter with 80 Hz cut-off (remote to low-pass cut-off to avoid transition band interference), in forward and reverse direction for zero phase delay.

Subsequently, rule-based algorithms were applied to the pulse waveforms' peaks (from Matlab function *findpeaks*) and zero-crossings to detect the relevant fiducials shown in Fig. 2d for an exemplary cardiac cycle phase. Briefly, starting from the ECG R-peak, the maximum in the first derivative was detected, indicating the pulse upstroke. Its adjacent zero-crossings were defined as diastolic and systolic pressures and diameters in the BP and distension waveform, respectively. The local maximum in the second derivative preceding the upstroke was defined as systolic foot of the distension (SF_D) and PPG (SF_{PPG}) waveforms [13]. In turn, the first maximum in the second derivative preceding SF_D was defined as start of the isovolumic contraction SIC, here propagated to the carotid artery [26], [36]. All fiducial markers involving peak detection were enhanced by quadratic peak interpolation to achieve subsample temporal accuracy at tenfold resolution, i.e. 200 μs.
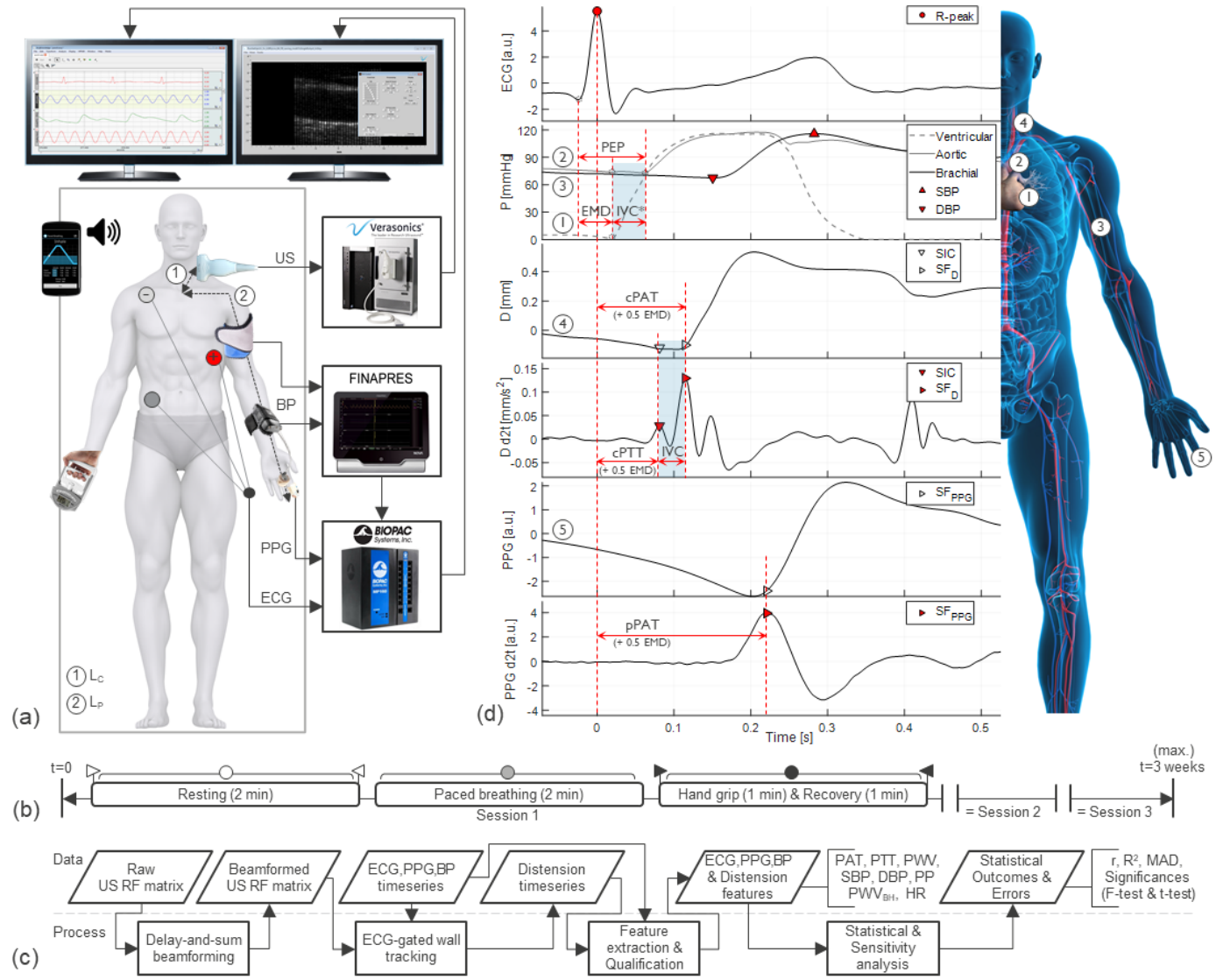
Fig. 2. Overview of methods. (a) Experimental setup with human subject in supine position. Utilities, sensors, and anthropometric distances indicated. (b) Experimental protocol timeline spanning three sessions over three weeks. Circle and triangle markers indicate continuous and intermittent data samples, respectively, and correspond to scatterplot markers in Figure 5. (c) Flow diagram for processing and analysis, separated by data and processes. (d) Exemplary cardiac cycle phase with signals, fiducials and intervals. Red markers indicate fiducial detection with transparent markers projecting to other signals. Isovolumic contraction highlighted as actual interval (IVC*) manifesting in aortic pressure waveform, and as propagated to carotid distension waveform (IVC) used for pulse arrival time segmentation. Central pulse transit time is indicated as the defined segment from the central pulse arrival time interval. Circled numbers mapping signal origin to the respective anatomic location.

c = central (prefix); (D|S)BP = (diastolic | systolic) blood pressure; d2t = second derivative; D = distension; ECG = electrocardiogram; EMD = electromechanical delay; HR = heart rate; IVC = isovolumic contraction; L_C = central arterial path length; L_P = peripheral arterial path length; MAD = mean absolute deviation; p = peripheral (prefix); P = pressure; PAT = pulse arrival time; PEP = pre-ejection period; PP = pulse pressure; PTT = pulse transit time; PPG = photoplethysmogram; $PWV_{(BH)}$ = (Bramwell-Hill) pulse wave velocity; r = correlation coefficient; R^2 = coefficient of determination; RF = radio frequency; SBP = systolic blood pressure; SF = systolic foot; SIC = start of isovolumic contraction; US = ultrasound; * = actual interval.

Fig. 2d shows the interval features computed from fiducial point timestamps (t). The distension-based central PAT was calculated as time difference between R-peak and SF_D, while accounting for the electromechanical delay (assumed constant at 40 ms and corrected by a factor 0.5 as partially comprised in the ECG Q-R interval), i.e.

$$cPAT = (t_{SF_D} - t_{R-peak}) - 0.5\,EMD. \quad (4)$$

The corresponding cPAT-based PWV was computed as

$$cPWV_{PAT} = \frac{2.5\,L_C}{cPAT} \quad (5)$$

with L_C corrected by a factor 2.5, devised from a 3D human model (Biodigital Inc., USA) to account for the underestimation of the actual arterial path length from left ventricle to common carotid artery (~0.5 in ventral and ~2 in cranial direction).

Rearranging Eq.3 for PTT yields

$$PTT = PAT - IVC - EMD. \quad (6)$$

The IVC manifestation in the ultrasound-based distension waveform was calculated as time difference between SIC and SF_D, respectively signaling the IVC onset and the aortic valve opening, i.e.

$$IVC = t_{SF_D} - t_{SIC}. \tag{7}$$

Combining Eq. 4, 6 and 7, we obtain the distension-based central PTT

$$cPTT = (t_{SF_D} - t_{R\text{-}peak}) - (t_{SF_D} - t_{SIC}) - 0.5\,EMD$$
$$= (t_{SIC} - t_{R\text{-}peak}) - 0.5\,EMD \tag{8}$$

and corresponding cPTT-based PWV

$$cPWV_{PTT} = \frac{2.5\,L_C}{cPTT}. \tag{9}$$

Similarly, we obtain the PPG-based peripheral PAT

$$pPAT = (t_{SF_{PPG}} - t_{R\text{-}peak}) - 0.5\,EMD \tag{10}$$

with corresponding pPAT-based PWV

$$pPWV_{PAT} = \frac{L_P}{pPAT}. \tag{11}$$

Heart rate (HR) was computed from R-R intervals and the Bramwell-Hill PWV (PWV_{BH}) from Eq.1 with pulse pressure (PP = SBP-DBP), substituting dP.

Features were qualified based on objective quality indicators. Initially, the features must comply with absolute and beat-to-beat variability thresholds to ensure that their values are within the physiologically valid range (Table provided as supplementary material). Accordingly, distension-based features must be valid for at least half the number of scanlines per cardiac cycle, with the final feature value being computed as mean of those valid. Regarding cumulative data, all features must be valid for at least half the number of cardiac cycles per intervention to be valid.

3) Statistical & Sensitivity Analysis

Table I provides an overview of all features entering the analyses. Continuous samples were defined as mean feature value per subject, session and intervention. Recovery after hand grip was excluded to avoid hysteresis of vascular compliance [43]. Similarly, intermittent samples corresponding to cuff BP were defined as mean of the 15 qualified cardiac cycles pre-, and post resting and hand grip. These samples entered a set of least squares linear regression analyses with SBP, DBP, PP, HR and PWV_{BH} as dependent variables y, and central and peripheral PAT, PTT and PWV quantities as independent variables x, respectively of the form $y = \beta x + \alpha$. Outcomes were the Pearson correlation coefficient (r), the coefficient of determination (R^2), the F-statistic for correlation significance, and the mean absolute deviation (MAD, i.e. mean of absolute residual errors). The MAD has a more balanced weighting than the conventional root mean

TABLE I
OVERVIEW OF FEATURES

Feature	Sensing modality	Brief description	Equation
cPAT, s	ECG & US	Interval from electromechanical cardiac onset to central vascular pulse wave (biased by IVC)	(4)
$cPWV_{PAT}$, m/s		cPAT converted to PWV over L_C	(5)
IVC, s	US	Interval from mechanical cardiac onset to aortic valve opening	(7)
cPTT, s	ECG & US	Interval from approximated aortic valve opening to central vascular pulse wave (presumably unbiased)	(8)
$cPWV_{PTT}$, m/s		cPTT converted to PWV over L_C	(9)
pPAT, s	ECG & PPG	Interval from electromechanical cardiac onset to peripheral vascular pulse wave (biased by IVC and heterogenous stiffness)	(10)
$pPWV_{PAT}$, m/s		pPAT converted to PWV over L_P	(11)
PWV_{BH}, m/s	US & BP	PWV reference based on arterial distensibility	(1)
SBP, mmHg	BP	Peak BP	-
DBP, mmHg	BP	Baseline BP	-
PP, mmHg	BP	Baseline-to-peak BP	-
HR, bpm	ECG	Heart rate based on R-R interval	-

c = central (prefix); (D|S)BP = (diastolic | systolic) blood pressure; HR = heart rate; IVC = isovolumic contraction; L_C = central arterial path length; L_P = peripheral arterial path length p = peripheral (prefix); PAT = pulse arrival time; PP = pulse pressure; PTT = pulse transit time; $PWV_{(BH)}$ = (Bramwell-Hill) pulse wave velocity; US = ultrasound.

squared error and furthermore serves as error metric in the IEEE BP validation standard (MAD ≤ 5 mmHg receives grade A and MAD ≥ 7 mmHg grade D) [44]. However, this merely concerns the error, while full standard compliance has more stringent requirements on the subject population and reference BP. To test MAD differences between predictors, paired-sample t-tests for mean equality were conducted.

In addition, a sensitivity analysis was conducted to simulate inaccuracies in arterial path length estimation, both alone and combined with simulated fiducial point detection noise. For this purpose, uniform white noise of 1 cm and 5 cm was added around the manually assessed distances L_C (9.5±1.5 cm) and L_P (87.4±7.6 cm), respectively simulating approximately 10% and 5% variability in path length. Likewise, noise of 5 ms was added around the fiducials to simulate misdetections up to twice the sampling interval. Noise was added simultaneously to all subjects in 100 variations, yet randomly per subject.

III. RESULTS

A. Qualification & Overview

Overall, fiducial detection and feature extraction showed a good reproducibility. After qualification, 87% of the data was preserved, corresponding to 78 of 90 continuous and 104 of 120 intermittent samples. Disqualified data consisted of one subject systematically exhibiting a high degree of lateral carotid artery displacement, making SIC unidentifiable, and random datapoints among the remainders, respectively accounting for 10% and 3% of the discarded data.
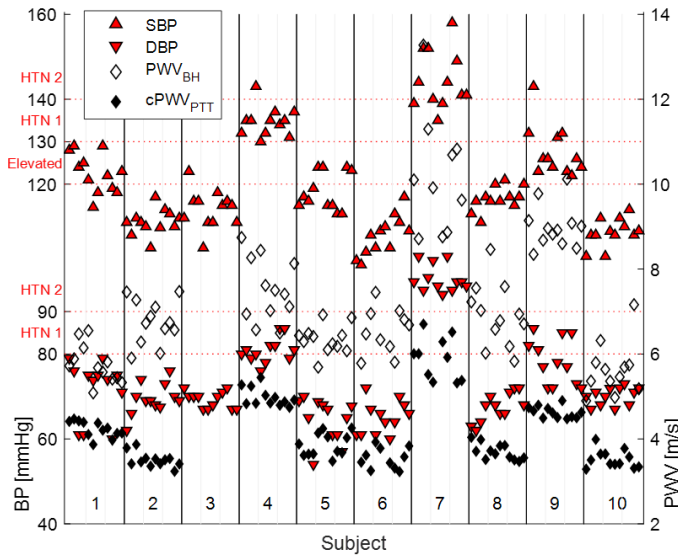
Fig. 3: Overview of all subjects and sessions with intermittent systolic (SBP) and diastolic blood pressure (DBP), corresponding central pulse transit time-based pulse wave velocity (cPWV_PTT) and Bramwell-Hill pulse wave velocity (PWV_BH). For disqualified samples neither PWV is included. Dashed lines indicate stage 1 and 2 hypertension (HTN) thresholds.

Figure 3 gives an overview of all subjects with intermittent samples (expecting 4 per session, thus 12 in total) of BP and corresponding PWV measurements (PWV$_{BH}$) and estimations (cPWV$_{PTT}$). PWV$_{BH}$ ranges from 5 to 13 m/s and BP from normotension to stage 2 hypertension [45]. Fundamental relations between the displayed quantities are apparent from visual inspection, with cPWV$_{PTT}$ systematically lower and exhibiting a narrower range compared to PWV$_{BH}$.

B. Signals & Features

Fig. 4 gives a typical intra-subject example of the paced breathing intervention with SBP as beat-to-beat timeseries and in response to interval features. PWV$_{BH}$ is in close coherence with SBP as mutual changes are widely determined here by respiratory induced PP variation. The expectedly negative correlation between PAT and SBP is stronger for the peripheral (pPAT, r = -0.55) than the central path (cPAT, r = 0.09). Evidently, the relatively weak cPAT correlation is caused by the expectedly positive relation between IVC and SBP (r = 0.6), masking the strongest correlation between SBP and the central PTT (cPTT, r = -0.66). This phenomenon is further driven by the relatively high IVC contribution to cPAT (43/115 ms) as compared to pPAT (43/230 ms), being approximately doubled (19% vs. 37%) in this example.

C. Regression, Sensitivity & Error Analysis

Fig. 5 shows an excerpt of the linear regression analysis with continuous and intermittent PWV$_{BH}$ responses to estimated PWV predictors. Analogically to Fig. 5a&b, an overall congruence between the continuous and intermittent data was found across all predictors and responses, and irrespective of the paced breathing intervention comprised by the continuous data only. Therefore, the presented results focus on intermittent PWV$_{BH}$ and BP obtained from the gold standard reference. Furthermore, from Fig.5b-d it is evident that cPWV$_{PTT}$ correlates substantially higher with PWV$_{BH}$ compared to central (cPWV$_{PAT}$) and peripheral (pPWV$_{PAT}$) PAT-based PWV (R^2 = 0.56 vs. 0.35 vs. 0.27). However, cPWV$_{PTT}$ was also found to systematically underestimate PWV$_{BH}$ (Δμ: 2.9 m/s; Δσ: 0.7 m/s).
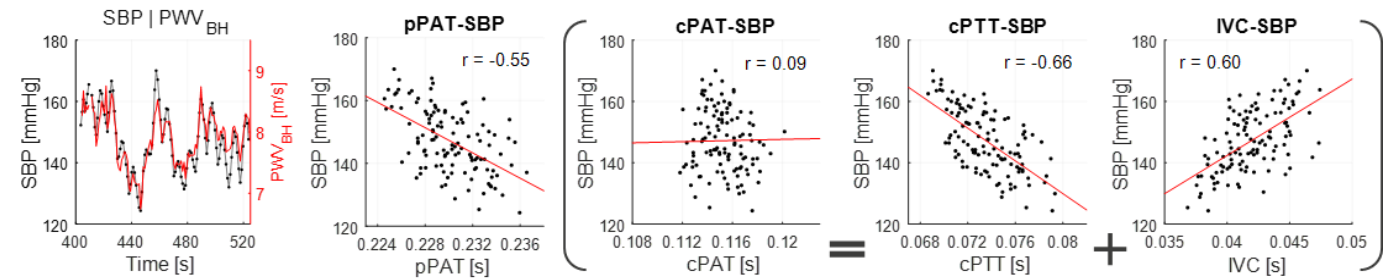

Fig. 4. Typical example of intra-subject recording throughout the paced breathing intervention. Timeseries signals of systolic blood pressure (SBP) and Bramwell-Hill pulse wave velocity (PWV$_{BH}$) in leftmost plot. Scatterplots display the correlations between interval features and SBP (quasi PWV$_{BH}$).
c = central (prefix); IVC = isovolumic contraction; p = peripheral (prefix); PAT = pulse arrival time; PTT = pulse transit time; r = correlation coefficient; PWV$_{BH}$ = Bramwell-Hill pulse wave velocity; SBP = systolic blood pressure.
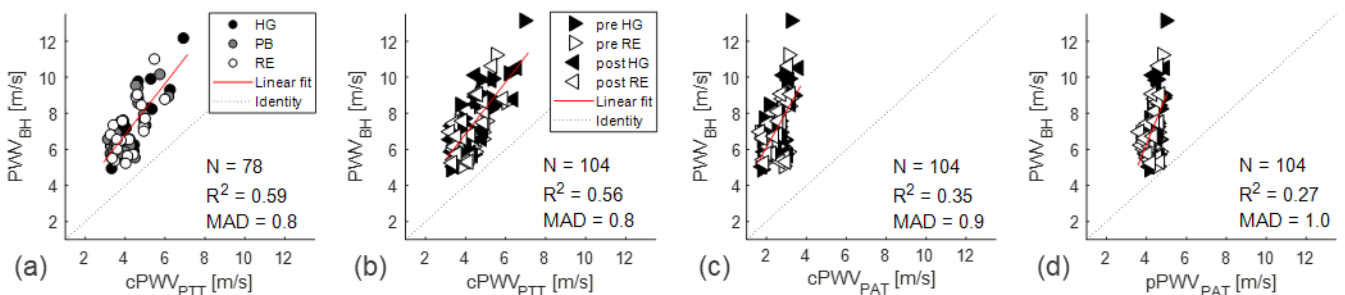

Fig. 5. Regression analyses for continuous (a) and intermittent (b-d) Bramwell-Hill pulse wave velocity (PWV$_{BH}$) responses to PWV predictors based on central pulse transit time cPWV$_{PTT}$ (a&b), central pulse arrival time cPWV$_{PAT}$ (c) and peripheral pulse arrival time pPWV$_{PAT}$ (d).
c = central (prefix); HG = hand grip; MAD = mean absolute deviation; N = number of samples; PB = paced breathing; p = peripheral (prefix); PWV$_{(BH |PAT| PTT)}$ = (Bramwell-Hill | pulse arrival time | pulse transit time) pulse wave velocity; R^2 = coefficient of determination; RE = resting.
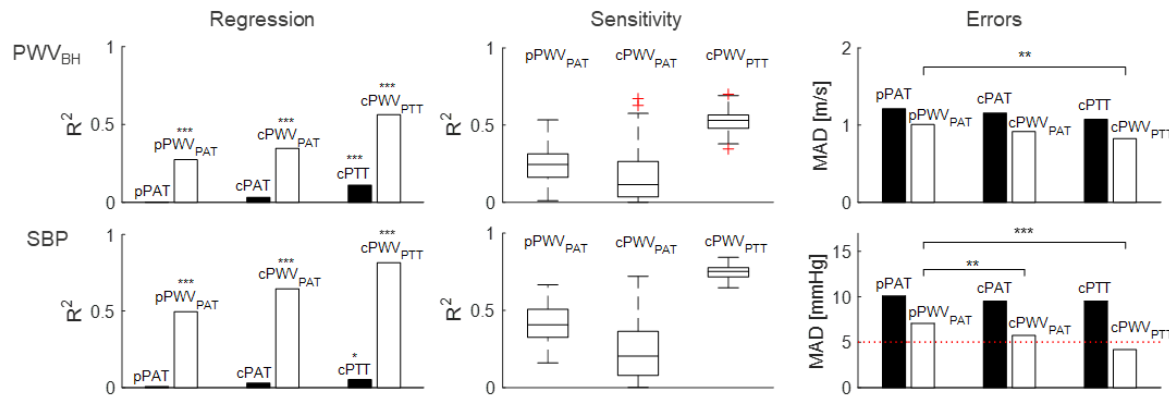
Fig. 6. Regression bar charts (left), sensitivity boxplots for path length variability (center) and MAD error bar charts (right), respectively for PWV_{BH} (top row) and SBP (bottom row, here with MAD threshold of 5 mmHg). * P < 0.05, ** P < 0.01, *** P < 0.001. F-statistic for correlation. Paired-sample t-test for MAD.
c = central (prefix); MAD = mean absolute deviation; p = peripheral (prefix); PAT = pulse arrival time; PTT = pulse transit time; $PWV_{(BH \mid PAT \mid PTT)}$ = (Bramwell-Hill | pulse arrival time | pulse transit time) pulse wave velocity; R^2 = coefficient of determination; SBP = systolic blood pressure.

Fig. 6 highlights the comparative results of the regression, sensitivity and error analyses, with complementary numerical details and further response variables presented in Table II. Similar to PWV_{BH}, $cPWV_{PTT}$ excelled any other predictor and showed the highest correlations with SBP (R^2 = 0.82) and DBP (R^2 = 0.66), while $cPWV_{PAT}$ was the strongest predictor for PP (R^2 = 0.36). The systematically lower R^2 found for PAT and PTT compared to PWV is not exclusively due to the 1/x transformation applied for PWV computation, but mainly attributed to the subject-specific path length information. For PWV_{BH}, SBP and DBP, R^2 gradually increased towards a more central and unbiased time interval predictor, becoming significant only for cPTT. Relating to this, the IVC duration (37±8 ms) accounted for 17% of pPAT and 32% of cPAT on average. For SBP and DBP, the β regression coefficients indicate the expected nonlinearity in the relation with PWV. HR did not significantly correlate with any cPWV, but showed significant correlations with $pPWV_{PAT}$ and all intervals,

particularly pPAT (R^2 = 0.49, P < .001).

The center boxplots in Fig. 6 reveal the sensitivity to the simulated path length variability, for which $cPWV_{PTT}$ shows an outstanding robustness with the highest and narrowest R^2 distribution for PWV_{BH} and similar tendencies for SBP. Correlations slightly deteriorated when fiducial detection noise was simulated in addition to path length variability, while the outstanding robustness of $cPWV_{PTT}$ was preserved.

The right bar charts in Fig. 6 show the results of the error analysis with significantly lower errors in both PWV_{BH} (P < .01) and SBP (P < .001) for $cPWV_{PTT}$ with respect to pPWV. For SBP and DBP, $cPWV_{PTT}$ even undercuts the IEEE standard threshold of 5 mmHg. Corresponding errors for the PAT and PTT interval predictors remain almost unaltered.

For the sake of completeness, PWV was also estimated from (fractions of) body height, but correlations were found to lie between those from PTT intervals and PWV from specific distances, and insufficient to meet the IEEE error margins.

TABLE II
RESULTS OF REGRESSION, SENSITIVITY AND ERROR ANALYSES
FOR INTERMITTENT PREDICTOR (HORIZONTAL) AND RESPONSE (VERTICAL) VARIABLES

		pPAT, s (.221 ± .019)	$pPWV_{PAT}$, m/s (4.3 ± 0.3)		cPAT, s (.114 ± .010)	$cPWV_{PAT}$, m/s (2.5 ± 0.5)		cPTT, s (.077 ± .007)	$cPWV_{PTT}$, m/s (4.2 ± 0.8)	
Regression		R^2	R^2	β	R^2	R^2	β	R^2	R^2	β
PWV_{BH}, m/s	(7.1 ± 1.5)	.00	.27***	2.7	.03	.35***	2.0	.11***	**.56*****	1.4
SBP, mmHg	(121 ± 12)	.01	.50***	29.5	.03	.65***	21.8	.05*	**.82*****	13.9
DBP, mmHg	(73 ± 10)	.01	.32***	19.9	.03	.32***	13.0	.18***	**.66*****	10.5
PP, mmHg	(47 ± 8)	.08**	.16***	10.8	.00	**.36*****	10.6	.06*	.17***	4.1
HR, bpm	(67 ± 9)	**.49*****	.18***	14.2	.29***	.01	2.5	.31***	.04	2.5
Sensitivity, R^2			$[Q_1, median, Q_3]$			$[Q_1, median, Q_3]$			$[Q_1, median, Q_3]$	
PWV_{BH}	Path length noise		[.16, .24, .31]			[.03, .11, .26]			**[.48, .53, .56]**	
	+ Fiducial noise		[.08, .15, .22]			[.01, .03, .09]			**[.41, .48, .54]**	
Error, MAD										
PWV_{BH}, m/s		1.2	1.0		1.2	0.9		1.1	**0.8****	
SBP, mmHg		10.1	7.1		9.5	5.7**		9.5	**4.2*****	
DBP, mmHg		7.9	6.4		7.6	6.5		7.4	**4.8*****	

Variable ranges indicated as (μ ± σ). * P < 0.05, ** P < 0.01, *** P < 0.001. F-statistic for correlation. Paired-sample t-test for MAD. Highest R^2 (Regression and Sensitivity) and lowest MAD error in **bold**, per row.
c = central (prefix); (D|S)BP = (diastolic | systolic) blood pressure; HR = heart rate; MAD = mean absolute deviation; p = peripheral (prefix); PAT = pulse arrival time; PP = pulse pressure; PTT = pulse transit time; $PWV_{(BH \mid PAT \mid PTT)}$ = (Bramwell-Hill | pulse arrival time | pulse transit time) pulse wave velocity ; $Q_{(1|3)}$ = (first | third) quartile; R^2 = coefficient of determination.

IV. DISCUSSION

In the present study, we demonstrate an approximation of central pulse wave velocity by segmenting pulse arrival time into the cardiac isovolumic contraction and central pulse transit time intervals, based on ultrasound carotid distension waveforms. In our repeated measurements design, considering intra- and inter-subject physiological variability and technical reproducibility we could confirm our hypothesis, that a central pulse wave velocity estimate yields superior correlations with Bramwell-Hill pulse wave velocity and blood pressure compared to conventional peripheral pulse arrival time. The observed improvements resulted from a combination of 1) measuring over a central arterial path, 2) segmenting pulse arrival time into vascular pulse transit time by eliminating isovolumic contraction and 3) converting into pulse wave velocity using estimated path lengths.

A. Validity IVC & PWV

Segmentation of PAT into cardiac IVC and vascular PTT was done using the SIC fiducial in the carotid distension waveform (Fig. 2d). The contribution of IVC to PAT was on average twice as large for the central compared to the peripheral site. Consequently, the sensitivity analysis showed large susceptibility of $cPWV_{PAT}$ to variations in arterial path length, which virtually amplify the unexplained IVC variability in PAT. While a more robust $pPWV_{PAT}$ (5% variability; relatively long path and low IVC contribution) tended to outperform $cPWV_{PAT}$ (10% variability; relatively short path and high IVC contribution), $cPWV_{PTT}$ demonstrated a clearly higher and less dispersed R^2. This suggests that for PWV computation a proper IVC isolation is more relevant than the critical path length accuracy causing up to 30% PWV variation alone, even in the rather robust carotid-femoral PWV [46]. In contrast, our distance measures and the corrective factor 2.5 for L_C appear as valid assumptions.

The values obtained for $cPWV_{PTT}$ were furthermore the closest in line with literature values expected for young to middle-aged cohort in consideration of a generic age-dependency [46]. The average IVC of 37 ms was marginally lower than expected from literature [26]. However, this may be attributed to this specific study (cohort, interventions, etc.), since the validity of SIC against invasive gold standard measurements was previously demonstrated [36].

B. Preceding Research Revisited

A recent study concluded that peripheral PAT (to finger or toe) is an accurate approximation of PTT at rest due to low PEP variability [47]. This may hold for intra-subject comparison, but for conversion to PWV this assumption should be treated with caution, considering both the arterial path length and hemodynamic mechanisms involved. For instance, previous studies found HR as a secondary predictor for BP alongside PAT in multivariate regression [48], [49]. However, we only observed a significant correlation between HR and pPWV but neither cPWV, which may be explained by different degrees of (inter-subject) sympathetic nervous activity, triggering peripheral vasoconstriction simultaneous to increased HR. In this case, HR may be considered as collinear

variable in a location specific model. However, there is still a lack of consensus on BP-independent HR-PWV interaction, which requires more thorough intra-subject research first [50].

Though results vary across literature, a much-cited study found significant correlations between PAT and SBP as well as PTT (obtained from impedance cardiography-based PAT segmentation) and DBP, but not vice versa, in various pharmacological interventions [28]. However, the only drug not supporting the PTT-SBP correlation was Salbutamol, causing peripheral vasodilation. Thus, the absence of a significant correlation between PTT, terminating at the index finger, and SBP would be explained by peripheral stiffness modulation. Thus, these findings are also location-specific and point to the importance of contextual interpretation. Accordingly, a PTT correlating with both DBP and SBP is expected and in line with our findings discussed hereafter.

C. PWV Correlations – PWV_{BH}

Regarding PWV_{BH}, the observed correlation with $cPWV_{PTT}$ as central PWV approximation (unbiased by IVC and based on homogenous stiffness) is intuitive as both quantities supposedly represent a central arterial stiffness. However, in spite of the significant correlation, 44% of PWV_{BH} variability remains unexplained and $cPWV_{PTT}$ systematically underestimates PWV_{BH} by approximately 3 m/s, which may be explained by three limitations of the deployed PWV_{BH}.

Firstly, PWV_{BH} is calculated from brachial pulse pressure and, due to peripheral pulse pressure amplification, likely to overestimate the true central PWV [1]. Importantly, the degree of pulse pressure amplification varies between individuals depending on age and overall cardiovascular constitution [51]. Thus, the (reconstructed) brachial pulse pressure may cause PWV_{BH} to deviate differently from true central PWV between subjects. Secondly, the Bramwell-Hill equation assumes a linear pressure-volume relation over the full diastolic-to-systolic changes. Considering the true nonlinear relation, systematic overestimation of distensibility-based PWV is expected compared to transit-time PWV obtained at diastolic level [50]. Moreover, different degrees of nonlinearity across subjects may contribute to the observed variability. Overall, $cPWV_{PTT}$ may reflect true central PWV more closely than PWV_{BH}, given the significant correlations, yet lower absolute values and less fluctuations (Fig. 3). Further validation of our method should therefore comprise a true central PWV reference or a suitable calibration technique [52].

D. PWV Correlations – BP

The highest correlations among the BP response variables were observed for SBP and not DBP, which is remarkable considering that PWV was measured at DBP level [53]. In that sense, it is important to realize that arterial compliance, strongly related to (diastolic) arterial stiffness, determines the pressure increase over the cardiac cycle due to the ejected stroke volume. This means that in subjects with similar DBP and stroke volume, yet different diastolic arterial stiffness, a correlation between PWV and SBP is likely expected. Indeed, this is in line with the understanding of large artery stiffening as most important determinant of systolic hypertension and

age-dependent PP increase due to loss of elastic cushioning and earlier wave reflections [1], [46]. Thus, higher diastolic PWV, implying higher intrinsic stiffness, is expected to project to higher SBP due to loss of arterial distensibility.

Essentially linear relationships between PWV and both DBP and SBP were observed, although the β coefficients suggest a nonlinearity from DBP to SBP level. This piecewise linearity per BP level could be explained by 1) individual offsets with more discernible intra-subject nonlinearities, 2) the predominantly young to middle-aged cohort characterized by a more linear pressure-volume relation or 3) more linear models proposed as alternative to Moens-Korteweg, e.g. the Fung hyperelastic model [54], which further indicates that there is no clear consensus yet as to the degree of linearity.

The highest correlation with PP was observed for $cPWV_{PAT}$, which may be explained by the comprised IVC information, hence an interdependency of contractility and PP [55]. However, a positive β coefficient shows that this correlation is still driven by PTT rather than IVC.

E. Modelling, Statistics & Study Design

We deliberately used a first principles 'white box' approach to investigate the relations between different PWV estimates and BP, starting from the fundamental physiological quantities involved. This stands in contrast to a data-driven 'black box' approach wherein available quantities are combined in multivariate regression or machine learning models. In this way, we identified a key marker leading to less biased estimates of central PWV. Furthermore, the significant correlations obtained seemingly hold for a rather generic population without applying secondary predictors, grouping or extensive calibration; only exception being a personalization step using the rather accessible distance measure L_C. Although the repeated measurements validate consistency of the obtained statistics, the prospective development of clinically valid estimation models should be based on unbiased cross validation with separated training and testing data.

Regarding the validity of the presented results, the response variables showed adequate ranges for a proof-of-concept study. Although PWV_{BH} was slightly less balanced than BP, we obtained normally distributed and heteroscedastic residual errors, which renders the regression analyses essentially valid. Whereas the present study was confined to a non-patient cohort, future research should include larger patient groups of clinical relevance, i.e. different phenotypes of vascular aging and hypertension, to validate our approach in full compliance with the ARTERY PWV standard and the IEEE BP standard, respectively [44], [56]. In addition, specific patient groups may be included to further evaluate the robustness of our approach, e.g. those with variations in EMD due to atrial fibrillations [57]. Also, dynamic exercise or pharmacological interventions may be conducted to respectively obtain larger and more versatile intra-subject variation in PWV and BP.

F. Instrumentation & Processing

Wherever applicable, we followed best practices to obtain valid PWV, e.g. by using the sternal notch as anatomic landmark for arterial path length estimation [56] or by using the second derivative maximum for robust systolic foot fiducial timings, instead of the intersecting tangent method or similar [13], [58]. Our approach essentially depends on identifiability of the SIC fiducial, which may be compromised by (a combination of) physiological causes and technical limitations, e.g. in case of the disqualified subject with abnormal carotid artery motion. In this case, more advanced image processing algorithms could ensure the required stability [59]. Besides, diminished prominence of SIC was observed in older subjects, which may be attributed to a loss myocardial contraction velocity [60]. In contrast, increased vascular stiffness as another age-dependent phenomenon may also promote the propagation of waveform features due to lower damping in the mechanical coupling between heart, aorta and carotid artery in extension. This compromise should be further investigated in relevant cohorts to determine whether the absence of SIC (provided stable images) contraindicates our approach or might be an indication of increased vascular stiffness or cardiac dysfunction by itself.

G. Clinical Perspectives

In the present work, we provide proof-of-principle for a method to approximate central PWV with a strong predictive utility for BP, essentially from a single ultrasound-based arterial distension waveform combined with ECG and a readily accessible anthropometric distance. With the potential to reduce the ultrasound probe to a single M-line modality, the method may be translated to an image free technique and, with present advances for integration, even be scaled to a portable or wearable device [24], [61]. Moreover, ultrasound is versatile and provides information from deeper located arteries, whose pressure and stiffness are of major clinical interest in cardiovascular risk assessment as they reflect damage in both small and large arteries [1]. In addition, central SBP (and hence PWV) changes more drastically with age increments, wherefore it is not only of higher prognostic value than peripheral BP, but also an early indication for preventive measures [62]. In the future, our method may present a convenient single probe alternative to the rather impractical carotid-femoral PWV and perhaps, as oftentimes intended, an unobtrusive surrogate for BP monitoring. Although certain similarity in elastic properties between the carotid and central aortic artery may be assumed, a proper validation study should be conducted [56].

V. CONCLUSION

Cardiac isovolumic contraction onset as signaled in ultrasound-based carotid distension waveforms enables segmentation of pulse arrival time to obtain unbiased vascular pulse transit time. The corresponding pulse wave velocity estimates provide the basis for reliable single-site assessment of central arterial stiffness, confirmed by significant correlations with the established Bramwell-Hill pulse wave velocity and systolic blood pressure.

REFERENCES

[1] M. E. Safar *et al.*, "Interaction between hypertension and arterial stiffness an expert reappraisal," *Hypertension*, vol. 72, no. 4, pp. 796–805, 2018, doi: 10.1161/HYPERTENSIONAHA.118.11212.

[2] S. Laurent, P. Boutouyrie, P. G. Cunha, P. Lacolley, and P. M. Nilsson, "Concept of Extremes in Vascular Aging," *Hypertension*, vol. 74, no. 2, pp. 218–228, 2019, doi: 10.1161/hypertensionaha.119.12655.

[3] C. Vlachopoulos *et al.*, "Association of Estimated Pulse Wave Velocity With Survival," *JAMA Netw. Open*, vol. 2, no. 10, p. e1912831, 2019, doi: 10.1001/jamanetworkopen.2019.12831.

[4] T. Koivistoinen *et al.*, "Pulse Wave Velocity Predicts the Progression of Blood Pressure and Development of Hypertension in Young Adults," *Hypertension*, vol. 71, no. 3, pp. 451–456, 2018, doi: 10.1161/HYPERTENSIONAHA.117.10368.

[5] A. Tijsseling and A. Anderson, "A. Isebree Moens and DJ Korteweg: On the Speed of Propagation of Waves in Elastic Tubes," *Conf. Press. Surges*, no. December, 2012.

[6] J. Bramwell and A. Hill, "The velocity of the pulse wave in man," *Proc. R. Soc. Biol. Sci.*, vol. 93, pp. 298–306., 1922.

[7] B. Spronck *et al.*, "Pressure-dependence of arterial stiffness," *J. Hypertens.*, vol. 33, no. 2, pp. 330–338, 2015, doi: 10.1097/HJH.0000000000000407.

[8] D. H. Bergel, "The static elastic properties of the arterial wall," *J. Physiol.*, vol. 156, no. 3, pp. 445–457, 1961, doi: 10.1113/jphysiol.1961.sp006686.

[9] W. W. Nichols and D. G. Edwards, "Arterial elastance and wave reflection augmentation of systolic blood pressure: Deleterious effects and implications for therapy," *J. Cardiovasc. Pharmacol. Ther.*, vol. 6, no. 1, pp. 5–21, 2001, doi: 10.1177/107424840100600102.

[10] P. Salvi *et al.*, "Noninvasive Estimation of Aortic Stiffness Through Different Approaches," *Hypertens. (Dallas, Tex. 1979)*, vol. 74, no. 1, pp. 117–129, 2019, doi: 10.1161/HYPERTENSIONAHA.119.12853.

[11] G. Mancia, R. Fagard, R. E. S. Germany, P. Anton, and P. S. Uk, "2013 ESH / ESC Guidelines for the management of arterial hypertension," pp. 1281–1357, 2013, doi: 10.1093/eurheartj/eht151.

[12] B. Williams *et al.*, "2018 ESC/ESH Guidelines for the management of arterial hypertension," *Eur. Heart J.*, vol. 39, no. 33, pp. 3021–3104, Sep. 2018, doi: 10.1093/eurheartj/ehy339.

[13] E. Hermeling, K. D. Reesink, R. S. Reneman, and A. P. G. Hoeks, "Measurement of Local Pulse Wave Velocity: Effects of Signal Processing on Precision," *Ultrasound Med. Biol.*, vol. 33, no. 5, pp. 774–781, 2007, doi: 10.1016/j.ultrasmedbio.2006.11.018.

[14] A. Swillens, L. Taelman, J. Degroote, J. Vierendeels, and P. Segers, "Comparison of non-invasive methods for measurement of local pulse wave velocity using fsi-simulations and in vivo data," *Ann. Biomed. Eng.*, vol. 41, no. 7, pp. 1567–1578, 2013, doi: 10.1007/s10439-012-0688-z.

[15] E. Chung, G. Chen, B. Alexander, and M. Cannesson, "Non-invasive continuous blood pressure monitoring: a review of current applications.," *Front. Med.*, vol. 7, no. 1, pp. 91–101, Mar. 2013, doi: 10.1007/s11684-013-0239-5.

[16] R. Mukkamala *et al.*, "Toward Ubiquitous Blood Pressure Monitoring via Pulse Transit Time: Theory and Practice," *IEEE Trans. Biomed. Eng.*, vol. 62, no. 8, pp. 1879–1901, 2015, doi: 10.1109/TBME.2015.2441951.

[17] D. Buxi, J.-M. Redouté, and M. R. Yuce, "A survey on signals and systems in ambulatory blood pressure monitoring using pulse transit time," *Physiol. Meas.*, vol. 36, p. R1, 2015, doi: 10.1088/0967-3334/36/3/R1.

[18] X. R. Ding *et al.*, "Continuous Blood Pressure Measurement From Invasive to Unobtrusive: Celebration of 200th Birth Anniversary of Carl Ludwig," *IEEE J. Biomed. Heal. Informatics*, vol. 20, no. 6, pp. 1455–1465, 2016, doi: 10.1109/JBHI.2016.2620995.

[19] M. Elgendi *et al.*, "The use of photoplethysmography for assessing hypertension," *npj Digit. Med.*, no. June, pp. 1–11, 2019, doi: 10.1038/s41746-019-0136-7.

[20] K. Matsumura, P. Rolfe, S. Toda, and T. Yamakoshi, "Cuffless blood pressure estimation using only a smartphone," *Sci. Rep.*, vol. 8, no. 1, pp. 1–9, 2018, doi: 10.1038/s41598-018-25681-5.

[21] J. Lee, J. J. Sohn, J. Park, S. M. Yang, S. Lee, and H. C. Kim, "Novel blood pressure and pulse pressure estimation based on pulse transit time and stroke volume approximation," *Biomed. Eng. Online*, vol. 17, no. 1, pp. 1–20, 2018, doi: 10.1186/s12938-018-0510-8.

[22] S. L.-O. Martin *et al.*, "Weighing Scale-Based Pulse Transit Time is a Superior Marker of Blood Pressure than Conventional Pulse Arrival Time," *Sci. Rep.*, vol. 6, no. October, p. 39273, 2016, doi: 10.1038/srep39273.

[23] W. Chen, T. Kobayashi, S. Ichikawa, Y. Takeuchi, and T. Togawa, "Continuous estimation of systolic blood pressure using the pulse arrival time and intermittent calibration," *Med. Biol. Eng. Comput.*, vol. 38, no. 5, pp. 569–574, Sep. 2000, doi: 10.1007/BF02345755.

[24] C. Wang *et al.*, "Monitoring of the central blood pressure waveform via a conformal ultrasonic device," *Nat. Biomed. Eng.*, vol. 2, no. 9, pp. 687–695, 2018, doi: 10.1038/s41551-018-0287-x.

[25] J. Krohova, B. Czippelova, Z. Turianikova, Z. Lazarova, I. Tonhajzerova, and M. Javorka, "Preejection period as a sympathetic activity index: A role of confounding factors," *Physiol. Res.*, vol. 66, no. 2, pp. S265–S275, 2017.

[26] K. D. Reesink, E. Hermeling, M. C. Hoeberigs, R. S. Reneman, and A. P. Hoeks, "Carotid artery pulse wave time characteristics to quantify ventriculoarterial responses to orthostatic challenge," *J Appl Physiol*, vol. 102, no. 6, pp. 2128–2134, 2007, doi: 10.1152/japplphysiol.01206.2006.

[27] G. Cybulski, *Ambulatory Impedance Cardiography*, vol. 76. Berlin, Heidelberg: Springer Berlin Heidelberg, 2011.

[28] R. a Payne, C. N. Symeonides, D. J. Webb, and S. R. J. Maxwell, "Pulse transit time measured from the ECG: an unreliable marker of beat-to-beat blood pressure.," *J. Appl. Physiol.*, vol. 100, no. 1, pp. 136–41, Jan. 2006, doi: 10.1152/japplphysiol.00657.2005.

[29] G. Zhang, M. Gao, D. Xu, N. B. Olivier, and R. Mukkamala, "Pulse arrival time is not an adequate surrogate for pulse transit time as a marker of blood pressure.," *J. Appl. Physiol.*, vol. 111, no. 6, pp. 1681–6, Dec. 2011, doi: 10.1152/japplphysiol.00980.2011.

[30] A. D. Wiens and O. T. Inan, "Accelerometer body sensor network improves systolic time interval assessment with wearable ballistocardiography," *Proc. Annu. Int. Conf. IEEE Eng. Med. Biol. Soc. EMBS*, vol. 2015-Novem, pp. 1833–1836, 2015, doi: 10.1109/EMBC.2015.7318737.

[31] O. T. Inan *et al.*, "Ballistocardiography and Seismocardiography: A Review of Recent Advances," *IEEE J. Biomed. Heal. Informatics*, vol. 19, no. 4, pp. 1414–1427, 2015, doi: 10.1109/JBHI.2014.2361732.

[32] D. Buxi, "Systolic Time Interval Estimation using Continuous Wave Radar with On-body Antennas," *IEEE J. Biomed. Heal. Informatics*, vol. 2194, no. c, pp. 1–1, 2017, doi: 10.1109/JBHI.2017.2731790.

[33] M. Pour Ebrahim *et al.*, "Blood Pressure Estimation Using On-body Continuous Wave Radar and Photoplethysmogram in Various Posture and Exercise Conditions," *Sci. Rep.*, vol. 9, no. 1, p. 16346, 2019, doi: 10.1038/s41598-019-52710-8.

[34] P. Dehkordi *et al.*, "Comparison of Different Methods for Estimating Cardiac Timings: A Comprehensive Multimodal Echocardiography Investigation," *Front. Physiol.*, vol. 10, no. August, 2019, doi: 10.3389/fphys.2019.01057.

[35] M. J. Van Houwelingen, D. Merkus, M. Te Lintel Hekkert, G. Van Dijk, A. P. G. Hoeks, and D. J. Duncker, "Initiation of ventricular contraction as reflected in the aortic pressure waveform," *Physiol. Meas.*, vol. 33, no. 4, pp. 557–569, 2012, doi: 10.1088/0967-3334/33/4/557.

[36] M. J. van Houwelingen, P. J. Barenbrug, M. C. Hoeberigs, R. S. Reneman, and A. P. G. Hoeks, "The onset of ventricular isovolumic contraction as reflected in the carotid artery distension waveform," *Ultrasound Med. Biol.*, vol. 33, no. 3, pp. 371–378, 2007, doi: 10.1016/j.ultrasmedbio.2006.08.014.

[37] World Medical Association (WMA), "WMA Declaration of Helsinki- Ethical Principles," *World Med. Assoc.*, no. October 1975, pp. 29–32, 2013.

[38] I. Guelen *et al.*, "Validation of brachial artery pressure reconstruction from finger arterial pressure.," *J. Hypertens.*, vol. 26, no. 7, pp. 1321–7, 2008, doi: 10.1097/HJH.0b013e3282fe1d28.

[39] L. M. Van Bortel *et al.*, "Clinical applications of arterial stiffness, task force III: Recommendations for user procedures," *Am. J. Hypertens.*, vol. 15, no. 5, pp. 445–452, 2002, doi: 10.1016/S0895-7061(01)02326-3.

[40] J. Grythe, "Beamforming algorithms - beamformers," 2015.

[41] P. J. Brands, A. P. G. Hoeks, L. A. F. Ledoux, and R. S. Reneman, "A radio frequency domain complex cross-correlation model to estimate blood flow velocity and tissue motion by means of ultrasound," *Ultrasound Med. Biol.*, vol. 23, no. 6, pp. 911–920, 1997, doi: 10.1016/S0301-5629(97)00021-5.

[42] F. Beutel, L. Mansilla Valle, C. Van Hoof, and E. Hermeling, "P64 Carotid Artery Tracking with Automated Wall Position Resets Yields Robust Distension Waveforms in Long-term Ultrasonic Recordings," *Artery Res.*, vol. 25, no. Supplement 1, p. S106, 2020, doi: 10.2991/artres.k.191224.095.

[43] Q. Liu, B. Yan, C.-M. Yu, Y.-T. Zhang, and C. Poon, "Attenuation of Systolic Blood Pressure and Pulse Transit Time Hysteresis during Exercise and Recovery in Cardiovascular Patients.," *IEEE Trans. Biomed. Eng.*, no. c, Oct. 2013, doi: 10.1109/TBME.2013.2286998.

[44] IEEE Engineering in Medicine and Biology Society, "IEEE Standard for Wearable , Cuffless Blood Pressure Measuring Devices (1708™-2014)." 2014.

[45] P. K. Whelton *et al.*, "2017 ACC/AHA/AAPA/ABC/ACPM/AGS/APhA/ASH/ASPC/NMA/PC NA Guideline for the Prevention, Detection, Evaluation, and Management of High Blood Pressure in Adults: Executive Summary," *J. Am. Coll. Cardiol.*, vol. 71, no. 19, pp. 2199–2269, May 2018, doi: 10.1016/j.jacc.2017.11.005.

[46] F. U. S. Mattace-Raso *et al.*, "Determinants of pulse wave velocity in healthy people and in the presence of cardiovascular risk factors: 'establishing normal and reference values,'" *Eur. Heart J.*, vol. 31, no. 19, pp. 2338–2350, Oct. 2010, doi: 10.1093/eurheartj/ehq165.

[47] M. C. Kortekaas, M. H. N. Van Velzen, F. Grune, S. P. Niehof, R. J. Stolker, and F. J. P. M. Huygen, "Small intra-individual variability of the preejection period justifies the use of pulse transit time as approximation of the vascular transit," *PLoS One*, vol. 13, no. 10, pp. 1–13, 2018, doi: 10.1371/journal.pone.0204105.

[48] F. S. Cattivelli, "Noninvasive Cuffless Estimation of Blood Pressure from Pulse Arrival Time and Heart Rate with Adaptive Calibration," no. 1, pp. 115–120, 2009, doi: 10.1109/P3644.34.

[49] J. S. Kim, K. K. Kim, H. J. Baek, and K. S. Park, "Effect of confounding factors on blood pressure estimation using pulse arrival time.," *Physiol. Meas.*, vol. 29, no. 5, pp. 615–24, May 2008, doi: 10.1088/0967-3334/29/5/007.

[50] B. Spronck *et al.*, "Heart rate and blood pressure dependence of aortic distensibility in rats," *J. Hypertens.*, vol. Publish Ah, Aug. 2020, doi: 10.1097/HJH.0000000000002608.

[51] T. K. Waddell, A. M. Dart, T. L. Medley, J. D. Cameron, and B. A. Kingwell, "Carotid pressure is a better predictor of coronary artery disease severity than brachial pressure," *Hypertension*, vol. 38, no. 4, pp. 927–931, 2001, doi: 10.1161/hy1001.096107.

[52] L. M. Van Bortel *et al.*, "Non-invasive assessment of local arterial pulse pressure: comparison of applanation tonometry and echo-tracking.," *J. Hypertens.*, vol. 19, no. 6, pp. 1037–44, 2001, doi: 10.1097/00004872-200106000-00007.

[53] B. Spronck, A. P. Avolio, I. Tan, M. Butlin, K. D. Reesink, and T. Delhaas, "Arterial stiffness index beta and cardio-ankle vascular index inherently depend on blood pressure but can be readily corrected," *J. Hypertens.*, vol. 35, no. 1, pp. 98–104, 2017, doi: 10.1097/HJH.0000000000001132.

[54] Y. Ma *et al.*, "Relation between blood pressure and pulse wave velocity for human arteries," *Proc. Natl. Acad. Sci. U. S. A.*, vol. 115, no. 44, pp. 11144–11149, 2018, doi: 10.1073/pnas.1814392115.

[55] N. Stergiopulos and N. Westerhof, "Third Workshop on Structure and Function of Large Arteries : Part III Determinants of Pulse Pressure," *Hypertension*, vol. 32, pp. 556–559, 1998.

[56] I. B. Wilkinson *et al.*, "ARTERY Society guidelines for validation of non-invasive haemodynamic measurement devices: Part 1, arterial pulse wave velocity," *Artery Res.*, vol. 4, no. 2, pp. 34–40, Jun. 2010, doi: 10.1016/j.artres.2010.03.001.

[57] Y. Shingu *et al.*, "Left-ventricular electromechanical delay is prolonged in patients with postoperative atrial fibrillation," *Eur. J. Cardio-thoracic Surg.*, vol. 39, no. 5, pp. 684–688, 2011, doi: 10.1016/j.ejcts.2010.08.015.

[58] S. C. Millasseau, A. D. Stewart, S. J. Patel, S. R. Redwood, and P. J. Chowienczyk, "Evaluation of carotid-femoral pulse wave velocity: Influence of timing algorithm and heart rate," *Hypertension*, vol. 45, no. 2, pp. 222–226, 2005, doi: 10.1161/01.HYP.0000154229.97341.d2.

[59] Z. Gao *et al.*, "Motion Tracking of the Carotid Artery Wall from Ultrasound Image Sequences: A Nonlinear State-Space Approach," *IEEE Trans. Med. Imaging*, vol. 37, no. 1, pp. 273–283, 2018, doi: 10.1109/TMI.2017.2746879.

[60] H. J. Priebe, "The aged cardiovascular risk patient," *Br. J. Anaesth.*, vol. 85, no. 5, pp. 763–778, 2000, doi: 10.1093/bja/85.5.763.

[61] J. Joseph, R. Radhakrishnan, S. Kusmakar, A. S. Thrivikraman, and M. Sivaprakasam, "Technical Validation of ARTSENS-An Image Free Device for Evaluation of Vascular Stiffness," *IEEE J. Transl. Eng. Heal. Med.*, vol. 3, no. May, p. 1900213, 2015, doi: 10.1109/JTEHM.2015.2431471.

[62] A. P. Avolio *et al.*, "Role of pulse pressure amplification in arterial hypertension: experts' opinion and review of the data.," *Hypertension*, vol. 54, no. 2, pp. 375–83, Aug. 2009, doi: 10.1161/HYPERTENSIONAHA.109.134379.

VI. SUPPLEMENTARY MATERIALS

ABSOLUTE AND BEAT-TO-BEAT VARIABILITY THRESHOLDS FOR DEFINED PHYSIOLOGICAL RANGE

Feature	Minimum	Maximum	Variability
SBP, mmHg	80	220	10
DBP, mmHg	20	150	10
PP, mmHg	20	80	10
HR, bpm	30	220	35
PWV, m/s	1	15	1
pPAT, s	0.08	0.45	0.035
cPAT, s			
cPTT, s	0.04	0.12	0.015
IVC, s	0.02	0.06	0.01

Variability computed as absolute quantity change between beats ($|$beat$_i$ - beat$_{i-1}|$).

c = central (prefix); (D$|$S)BP = (diastolic $|$ systolic) blood pressure; HR = heart rate; IVC = isovolumic contraction; p = peripheral (prefix); PAT = pulse arrival time; PP = pulse pressure; PTT = pulse transit time; PWV = pulse wave velocity (all measures).